INORGANIC CHEMISTRY
FRONTIERS

RESEARCH ARTICLE

View Article Online
View Journal

Cite this: DOI: 10.1039/d5qi01630d

Exploring the interactions of *N*7-platinated guanosines with the hCNT3 transporter: a molecular dynamics study

Giada Ciardullo,[a] Federica de Castro,[b] Alessia Dodaro,[a] Mario Prejanò,[a] Asjad Ali,[b] Michele Benedetti,*[b] Francesco P. Fanizzi[b] and Tiziana Marino*[a]

The translocation of nucleosides across cellular membranes requires a specific category of integral membrane proteins, known as nucleoside transporters. These proteins are crucial for the absorption of endogenous nucleosides as well as nucleoside-derived pharmaceuticals, including antineoplastic drugs. This research examined the comparative dynamic behavior of [Pt(dien)(*N*7-dGuo)]$^{2+}$ (**1**), *cis*-[Pt(NH$_3$)$_2$Cl(*N*7-dGuo)]$^{+}$ (**2**), and *cis*-[Pt(NH$_3$)$_2$(H$_2$O)(*N*7-dGuo)]$^{2+}$ (**3**) (where dien = diethylenetriamine and dGuo = 5′-(2′-deoxy)-guanosine) platinated nucleosides in the human concentrative nucleoside transporter type 3 (hCNT3), utilizing molecular dynamics (MD) simulations. The membrane protein hCNT3 is involved in the cellular absorption of numerous therapeutic nucleoside derivatives used in the treatment of both viral infections and malignancies. These simulations facilitated the characterization of the ligand-binding site, underscoring the critical role of the transmembrane domain TM9 in promoting nucleoside translocation across the membrane and in determining the interaction of certain platinated nucleosides within the transporter channel. Overall, this work underscores the potential of platinum-based modifications to enhance antitumor therapies based on nucleoside analogues by synergistically targeting hCNT transporters, metabolic pathways of natural nucleosides, and DNA functionality. Notably, the latter interactions, in the case of complexes **2** and **3**, could also produce the classical 1,2-intrastrand cross-link lesions with DNA, which are considered responsible for the antitumor activity of cisplatin and analogous complexes. These considerations could lay the groundwork for new strategies aimed at developing antitumor drugs characterized by enhanced antitumor activity, selectivity for tumor cells, and reduced systemic side effects.

Received 1st August 2025,
Accepted 4th September 2025
DOI: 10.1039/d5qi01630d
rsc.li/frontiers-inorganic

Introduction

Nucleoside Transporters (NTs) are integral membrane proteins that facilitate the translocation of nucleosides, the fundamental building blocks of nucleic acids such as DNA and RNA, across cell membranes. These proteins play pivotal roles in various biological processes, including nucleotide salvage pathways,[1] signal transduction,[2] and the regulation of extracellular and intracellular nucleotide concentrations.[3] Dysfunctions or altered expressions of nucleoside transporters can result in a range of medical conditions. Changes in their expression can impact the efficacy of nucleoside-based chemotherapies,[4] while their dysfunction can lead to drug resistance.[5] Mutations in genes encoding nucleoside transporters have been implicated in a range of severe metabolic disorders, including H syndrome, pigmented hypertrichosis, and insulin-dependent diabetes mellitus,[6,7] evidencing their critical physiological role.

Nucleoside transport across cell membranes is mediated by two major families: the human Equilibrative Nucleoside Transporters (hENTs, SLC29 family) and the human Concentrative Nucleoside Transporters (hCNTs, SLC28 family).[8] Despite their structural differences, these two families share similar substrate specificities. ENTs operate as sodium-independent uniporters, facilitating the bidirectional transport of nucleosides across cell membranes along their concentration gradients without energy input. They lack definite prokaryotic orthologues and include four isoforms: ENT1 of the solute carrier (SLC) family 29 (SLC29A1), ENT2 (SLC29A2), ENT3 (SLC29A3), and ENT4 (SLC29A4).[9] Notably,

[a]*Dipartimento di Chimica e Tecnologie Chimiche, Università della Calabria, Via P. Bucci, 87036 Rende, Italy. E-mail: tiziana.marino65@unical.it*
[b]*Dipartimento di Scienze e Tecnologie Biologiche ed Ambientali, Università del Salento, Prov.le Lecce-Monteroni, Centro Ecotekne, I-73100 Lecce, Italy. E-mail: michele.benedetti@unisalento.it*

ENT1 and ENT2 are pivotal for the pharmacokinetics of antiviral and anticancer nucleoside analogs, whereas ENT3 and ENT4 are involved in intracellular transport and lysosomal function.

In contrast, CNTs[10,11] are evolutionarily conserved energy-dependent symporters that require an inwardly directed sodium- or proton-dependent coupling to actively transport nucleosides against their concentration gradients. This energy-dependent mechanism allows for intracellular accumulation of nucleosides crucial for DNA/RNA synthesis and cellular homeostasis. hCNT1 (SLC28A1), hCNT2 (SLC28A2), and hCNT3 (SLC28A3) represent the primary isoforms of human CNTs in the solute carrier (SLC) family 28. Among these three, hCNT3 is distinguished by its high transport efficiency. Indeed, it can intracellularly concentrate nucleosides ten times more efficiently than CNT1 or CNT2, due to its 2 : 1 ratio of Na^+ to nucleoside coupling. It is located on the apical membrane of the intestine and liver epithelia and is broadly expressed in tissues including the intestine, kidney, liver, and pancreas,[12] making it of particular interest for systemic nucleoside uptake and drug absorption.

hCNT3 is a transporter for both purine and pyrimidine nucleosides, while CNT1 and CNT2 prefer pyrimidine and purine nucleosides, respectively.[13] It plays a crucial role in drug response and the development of resistance to anticancer drugs. hCNT3 plays a crucial role in the chemotherapeutic strategies that utilize modified nucleosides, such as enhancing the uptake and transport of various antileukemic drugs, including cladribine and fludarabine, through the cell membrane.[14,15] Nucleoside analog drugs, such as gemcitabine and cytarabine, are dependent on nucleoside transporters for their entry into cancer cells. Inhibition of these transporters may impede the absorption of these drugs, diminishing their effectiveness and potentially resulting in drug resistance. One potential mechanism linking these transporters to cancer is the upregulation of nucleoside transporters in cancer cells, which facilitates the uptake of nucleosides essential for accelerated DNA synthesis and cellular proliferation. Inhibiting these transporters could potentially decrease the intracellular levels of nucleosides, thereby impeding cancer cell growth.[16]

To enhance the effectiveness of cancer treatments, a deeper understanding of how chemotherapeutic agents exert their action is essential. Platinum-based compounds, such as cisplatin, carboplatin, and oxaliplatin, remain the cornerstone of approximately half of all cancer treatment regimens,[17–20] underscoring their clinical relevance. Recent advances suggest that combining these potent agents with nucleic acids may lead to groundbreaking therapeutic strategies. Platinated nucleosides may offer an intriguing approach, potentially merging the cytotoxic impact of platinum drugs with the targeted functionality of nucleoside analogues (NAs) into the same molecule.[21,22]

Our previous studies demonstrated that *N*7-platinated guanosine derivatives can enter HeLa cells *via* Na^+-dependent concentrative transporters located at the plasma membrane.[23,24] Building on these insights, the current study explores the role of the hCNT3 nucleoside transporter,[14] one of the most efficient nucleoside transporters among the CNT family, in facilitating the cellular uptake of modified nucleosides based on *N*7-platinated guanosine derivatives, which have potential as antitumor/antiviral drugs.

In this context, three complexes of particular interest were selected for the present study. The $[Pt(dien)(N7\text{-dGuo})]^{2+}$ (**1**) complex (where dien = diethylenetriamine and dGuo = 5′-(2′-deoxy)-guanosine), has been extensively studied in previous works.[25–32] This complex serves as an established model for *N*7-platinated purines. Previous studies have highlighted its significance as an experimental prototype for understanding the chemical behaviour and mechanisms of interaction of platinated purines with cellular substrates, as well as their potential therapeutic properties. For instance, it has been demonstrated that the related model complex [Pt(dien)(*N*7-dGTP)] (where dGTP = 5′-(2′-deoxy)-guanosine triphosphate) can be recognized by DNA polymerases and incorporated into newly-synthesized DNA.[23–27]

Alongside this species, the chloro-species *cis*-$[Pt(NH_3)_2Cl(N7\text{-dGuo})]^+$ (**2**), originally studied for its antitumor activity by Hollis *et al.*,[33] has been recently reconsidered in our studies to better understand the mechanism of its proven antitumor activity.[24,28,29] Indeed, *cis*-$[Pt(NH_3)_2Cl(N7\text{-dGuo})]^+$ (**2**) could serve as a suitable precursor for other active metabolites that could be generated after administration, such as the here considered aquated *cis*-$[Pt(NH_3)_2(H_2O)(N7\text{-dGuo})]^{2+}$ (**3**) hydrolytic product.

Building on previous research on the binding site interactions between Taq DNA polymerase and three different *N*7-platinated deoxyguanosine triphosphates,[28] we conducted a Molecular Dynamics (MD) investigation to examine the platinated nucleosides $[Pt(dien)(N7\text{-dGuo})]^{2+}$ (**1**), *cis*-$[Pt(NH_3)_2Cl(N7\text{-dGuo})]^+$ (**2**), and *cis*-$[Pt(NH_3)_2(H_2O)(N7\text{-dGuo})]^{2+}$ (**3**) (see Scheme 1) as potential substrates for the hCNT3 transporter. To better understand the specificity of platinated nucleoside uptake by this *trans*-membrane transporter and its potential access to specific cell types and intracellular compartments, we also studied the canonical dGuo for comparison. Our explicit MD simulations on the hCNT3 with and without nucleosides allowed us to explore the effects of platinated nucleosides on the structural and dynamic behaviour of hCNT3, and to investigate its inhibition mechanism compared to dGuo natural nucleoside.

This computational approach provides valuable insights into how platinum coordination affects substrate binding, enzyme stability, and the fidelity of DNA replication. Understanding these mechanisms is essential for designing novel therapeutic agents that leverage both the cytotoxic properties of platinum complexes and the specificity of nucleotide incorporation. The structural features of the active site and the pathways for ligand access and release can significantly affect substrate selectivity in these types of proteins.

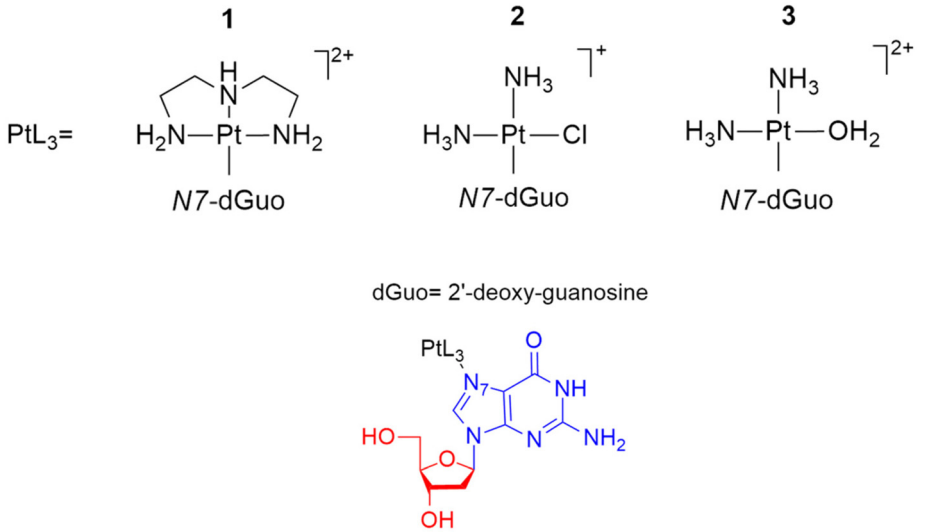

Scheme 1 Schematic representation of dGuo and platinated nucleosides $[Pt(dien)(N7\text{-}dGuo)]^{2+}$ (**1**), *cis*-$[Pt(NH_3)_2Cl(N7\text{-}dGuo)]^{+}$ (**2**), and *cis*-$[Pt(NH_3)_2(H_2O)(N7\text{-}dGuo)]^{2+}$ (**3**), (where dien = diethylenetriamine and dGuo = 5′-(2′-deoxy)-guanosine).

Methods

The structures of all the models are based on the human cryo-EM structure of the protein data bank (PDB) entry 6KSW,[34] with a resolution of 3.6 Å. This structure is in an inward-facing conformation. The structure of hCNT3 reveals a well-resolved density for residues 100-614, which can be divided into the central domain and additional N-terminal transmembrane (TM) helices. Each protomer of human CNT3 consists of 11 TMs, consistent with the expected topology of hCNTs. The central domain of hCNT3 resembles bacterial homologues and contains eight TMs, three interfacial helices (IH) and two hairpin helices (HP). The central domain is composed of two subdomains: the scaffold domain (TM4, TM5, TM6, TM9, IH2) and the transport domain (IH3, HP1, TM7, TM8, IH4, HP2, TM10, TM11). TM4 and TM5 are peripheral, while IH2, TM6 and TM9 form trimerization contacts between protomers. The transport domain has two structurally inverted repeats crucial for substrate recognition and alternate access, as supported by the evolutionary conservation analysis of CNTs.

The protein structure is composed of 632 amino acid residues and consists of three chains. The protein was utilized to construct five models, including the apo-form transporter and -dGuo, -$[Pt(dien)(N7\text{-}dGuo)]^{2+}$, -*cis*-$[Pt(NH_3)_2Cl(N7\text{-}dGuo)]^{+}$ and -*cis*-$[Pt(NH_3)_2(H_2O)(N7\text{-}dGuo)]^{2+}$ complexes. The nucleosides were designed using Gauss View[35] and are shown in Scheme 1. The guanines with platinum center were parametrized using MCPB.py[36] to generate frcmod and prepc files. Quantum mechanics calculations were performed using the Gaussian16 C.01 code[37] with the B3LYP functional and 6-31G* basis set.[38,39] The Seminario Method, implemented in the MCPB module of the Amber16 program,[40,41] was used for further analysis. Atomic charges were determined using the RESP approach, fitting the electrostatic potential according to the Merz–Singh–Kollman scheme.[42] The Amber16[43] modules Antechamber and Parmchk were utilized to generate necessary files for molecular mechanics (MM) relaxation of the complexes.

Next, the four nucleosides were subjected to molecular docking using Autodock 4 [43] on hCNT3 at the binding site of the transporter with the highest affinity. To generate the necessary PDBQT (Protein Data Bank, Partial Charge (Q), & Atom Type (T)) coordinate files for AutoGrid and AutoDock4 software, which include information on polar hydrogen atoms, partial charges, accurate atom types, and flexible molecule conformation, docking calculations were conducted to investigate the interaction between platinated guanines and the transporter. In ADT (Auto Dock Tools), Gasteiger-Marsili charges[44] were applied. The center of the grid box for each ligand was positioned on each chain of the transporter, with a box size of 126 × 126 × 126 $Å^3$. The pose with the lowest energy was selected for each system. Structural details about the binding mode of each molecule will be discussed in the next section.

In order to construct a model of the transporter systems within the cell membrane, we utilized CHARMM-GUI,[44] a web-based tool. The Membrane Builder option was employed to generate the necessary sequence of CHARMM inputs for constructing a protein/membrane complex and conducting molecular dynamics simulations. To mimic the composition of the plasma membrane, each model was embedded in a bilayer membrane system composed of the following components: phosphatidylcholine (23%), cholesterol (34%), sphingomyelin (17%), phosphatidylethanolamine (11%), and phosphatidylserine (8%).[45] The model was further solvated with TIP3P water molecules, which were positioned within 24 Å of the protein's matrix and cytoplasmic sides (see Fig. 1 for further details). The approximate number of atoms in each system were as follows: 58780 for the apo-form, 58812 for hCNT3-dGuo, 58833

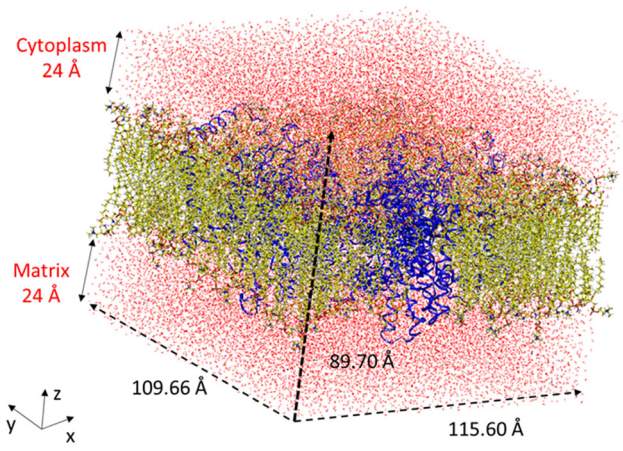

Species	CHARMM resname	Upper composition	Lower composition
Cholesterol	CHL1	34	34
Phosphatidylcholine	DLPC	23	23
Sphingomieline	PSM	17	17
Phosphatidylethanolamine	DLPE	11	11
Phosphatidylserine	DLPS	8	8

Fig. 1 Schematic representation of the model used in the molecular dynamics (MD) simulations for hCNT3, including the membrane. The composition of the membrane is also provided.

for hCNT3-[Pt(dien)(*N*7-dGuo)], 58822 for CNT3-*cis*-[Pt$(NH_3)_2$Cl(*N*7-dGuo)] and 58824 for hCNT3-*cis*-[Pt$(NH_3)_2(H_2O)$(*N*7-dGuo)]. To maintain electroneutrality, 91 Cl^- and 99 Na^+ counter ions were included. The final models were constructed using the CHARMM-GUI suite[44] in a rectangular box with dimensions of 89.70 × 109.66 × 115.60 $Å^3$. The AMBER force field was selected for the treatment of both the protein and lipid bilayer components (Lipid14 force field[46,47]).

To optimize each system, harmonic restraints were initially applied to the lipid molecules (50 kcal mol^{--1} $Å^{-2}$), followed by a second minimization step in which all atoms were unconstrained. The system was then subjected to a progressive heating process using the Langevin thermostat, starting at 0 K and reaching 298 K over a period of 10 ns, followed by 30 ns at 298 K. The production phase lasted 300 ns at 298 K. An integration step of 2 fs was used with the Berendsen barostat, and the SHAKE algorithm was employed in conjunction with the NPT ensemble and a pressure of 1 bar. The Particle Mesh Ewald summation method was utilized for calculating electrostatic potential, with long-range interactions accounted for up to a cutoff distance of 12 Å.

In order to identify any significant conformational changes, each system was simulated for 200 × 2 nanoseconds, resulting in a total simulation time of 2.0 μs. The simulations were performed using the GROMACS 2020 package.[48,49]

The primary modes of motion for hCNT3 in both systems are determined by the Principal Component Analysis (PCA) directions.[50] The PCA calculation used the simulations from each system as reference structures. Next, using the RMSD of hCNT3 in each system, the trajectories were projected into the corresponding first three principal components. The trajectories were then projected onto the first three principal components based on the RMSD of hCNT3 in each system. Additionally, correlation matrices were analyzed to show the correlated movements of hCNT3.

Results and discussion

In this study, we investigated model complexes consisting of guanosines coordinated to a platinum center at the *N*7 position. These complexes function as modified nucleosides with unchanged sugar moieties. Our research was guided by experimental evidence suggesting that *N*7-platinated purines may be able to enter cells through the plasma membrane of HeLa cervical cancer cells system, one of the cell models most used for preclinical studies on human cancer diseases.[25] The most relevant cellular uptake occurred with the $[Pt(dien)(N7\text{-dGuo})]^{2+}$. The results of our experiments indicate that *N*7-platination does not hinder the cellular uptake of nucleosides. Therefore, our focus was on the structural behavior observed in the binding site of hCNT3 and its surrounding area when interacting with the platinated nucleosides depicted in Scheme 1.

Protein–ligands interactions were explored to identify potential binding sites for nucleosides. Docking calculations of dGuo and species **1**, **2** and **3** within hCNT3 were performed. This step was necessary due to the absence of any structural evidence regarding the protein and the binding of the nucleosides. Interestingly, docking calculations revealed that a favourable binding pocket lies below TM9, representing inward-facing states of hCTN3 and nearby the intracellular solution, in agreement with structural information largely reported in the literature (Fig. 2).[34,51,52] Moreover, important residues for the recognition and transport of nucleosides, such as G340 and S374, are located in the binding pocket. Favourable binding energies resulted, ranging from −3.83 to −7.61 kcal mol^{-1} (see Table S1).

Lowest-energy conformations for the Pt-containing complexes were selected for subsequent MD simulations, in addition to hCNT3 in its apo-form and hCNT3 bound to the natural nucleoside dGuo.

The root-mean-square deviations (RMSDs) of the Cα atoms of the protein backbone were calculated for each MD trajectory, to assess the structural stability over the course of the simulations. The RMSD analysis showed that the apo-form system reached the equilibrium at 2.59 Å for most of the trajectory, similarly to the ligand-containing systems, which were centered at 2.46 Å (Fig. S1). This structural stability is further confirmed by principal components analysis, calculated for the protein components of each system (see Fig. S2). Moreover, being hCNT3 a Na^+-dependent protein, the presence of ions in proximity of the transporter was verified during the MD simulations, as confirmed by results in Fig. S3.

A homogeneous structural behavior was further evinced by analysis of root mean square fluctuations (RMSF) in Fig. 3, calculated for Cα atoms. Indeed, slight fluctuations of *ca.* 2 Å can be noticed for many amino acid residues of hCTN3. Four fluc-

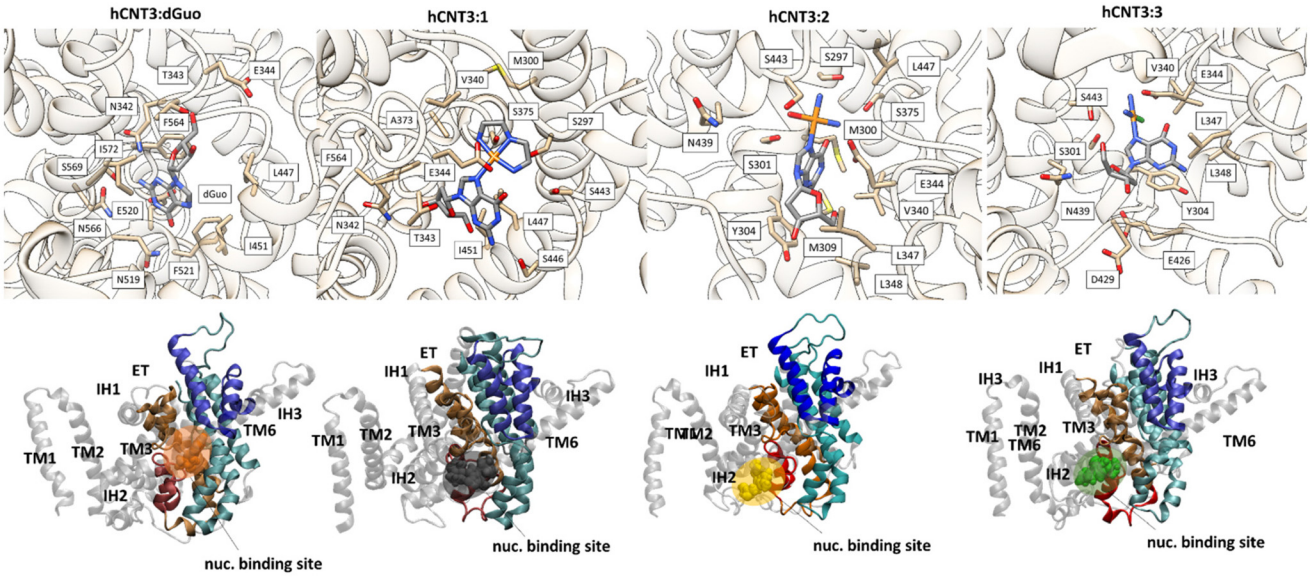

Fig. 2 Lowest energy docked poses of each ligand, used for molecular dynamics (MD) simulations, indicating their specific locations on the transporter. The following complexes are indicated in the picture: $[Pt(dien)(N7\text{-}dGuo)]^{2+}$ (**1**), *cis*-$[Pt(NH_3)_2Cl(N7\text{-}dGuo)]^{+}$ (**2**), and *cis*-$[Pt(NH_3)_2(H_2O)(N7\text{-}dGuo)]^{2+}$ (**3**), where dien = diethylenetriamine and dGuo = 5′-(2′-deoxy)-guanosine.

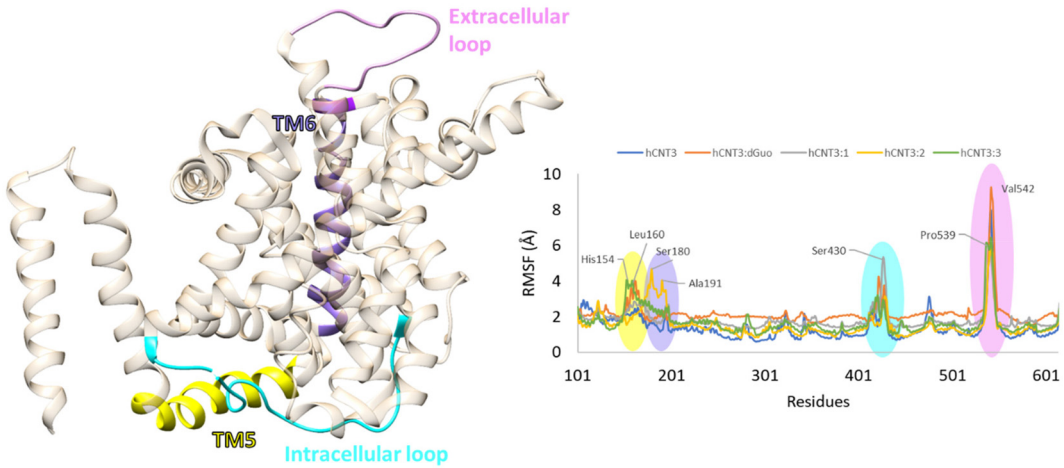

Fig. 3 Root mean square fluctuation (RMSF) calculated for the backbone atoms of the investigated systems. The peaks corresponding to the intracellular (green) and extracellular (purple) loops are circled. The residues corresponding to these peaks are highlighted. The following complexes are indicated in the picture: $[Pt(dien)(N7\text{-}dGuo)]^{2+}$ (**1**), *cis*-$[Pt(NH_3)_2Cl(N7\text{-}dGuo)]^{+}$ (**2**), and *cis*-$[Pt(NH_3)_2(H_2O)(N7\text{-}dGuo)]^{2+}$ (**3**), where dien = diethylenetriamine and dGuo = 5′-(2′-deoxy)-guanosine.

tuating secondary structures were identified, corresponding to the extra and intracellular loops (E536-S550 and T409-N432 sequences, respectively) and to TM5 and TM6 (see Fig. 3).

In the case of the loops, comparable values were obtained in each system, suggesting the inherent flexibility of these regions to favor the transport through the protein channel. Regarding TM5 and TM6, higher RMSF peaks resulted in complex **2** and **1**, respectively compared to complex **3**. Such fluctuations were generated by the shift of the species in the channel, which tended to be allocated in vicinal pockets within the protein. To study these interactions, the analysis started with detecting the number of hydrogen bonds formed between nucleosides and the membrane protein, for each system during the 2 × 200 ns of simulation (a donor–acceptor cutoff distance within 3.0 Å coupled to a maximum donor–hydrogen–acceptor angle of 20° was applied in the calculation). The follow-up is displayed as occupancy percentages of residues involved in the H-bonds in Fig. 4.

In the hCNT3:dGuo system, the most prevalent H-bonds involve the residues E344 (30.29%), T342 (27.11%), and E520 (24.92%), acting as acceptors, while multiple H-bonds are formed between the dGuo nucleoside, acting as an acceptor,

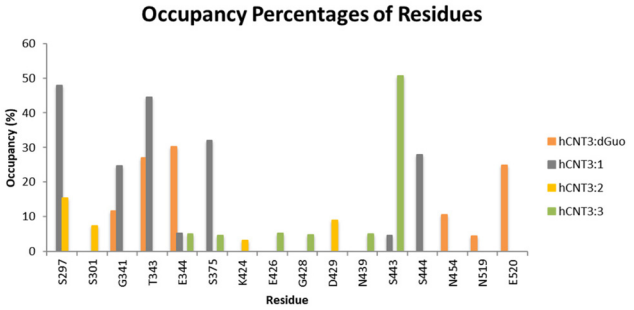

Fig. 4 Occupancy percentages of hCNT3 residues involved in H-bonds during the molecular dynamics (MD) simulation for dGuo, and [Pt(dien)(*N*7-dGuo)]$^{2+}$ (**1**), *cis*-[Pt(NH$_3$)$_2$Cl(*N*7-dGuo)]$^{+}$ (**2**), and *cis*-[Pt(NH$_3$)$_2$(H$_2$O)(*N*7-dGuo)]$^{2+}$ (**3**), species (where dien = diethylenetriamine and dGuo = 5′-(2′-deoxy)-guanosine).

and donor residues such as G341, suggesting a wide network of stabilizing interactions. In addition, N454 from TM9 also interacts with the dGuo moiety, albeit with a lower occupancy of 10.52% (see Fig. 4).

In the case of the Pt(dien)-containing system, more frequent hydrogen bond interactions were identified with the hydroxyl moiety of S297 and T343, with percentages of 47.95% and 44.55%, respectively. Similarly, the hCNT3:*cis*-[Pt(NH$_3$)$_2$(H$_2$O)(*N*7-dGuo)]$^{2+}$ system displays the highest occupancy of 50.67% for H-bond interaction with S443 of TM9 and the highest percentage of hCNT3:*cis*-[Pt(NH$_3$)$_2$Cl(*N*7-dGuo)]$^{+}$ is 15.18% for H-bond with the hydroxyl moiety of S297 (see Fig. 4).

Among the platinated systems, the [Pt(dien)(*N*7-dGuo)]$^{2+}$ (**1**) complex was found to be crucial in forming frequent and stabilizing H-bond interactions with the transporter. This complex generates highly stable interactions that can significantly affect the translocation of species **1** through the transporter channel in contrast to the nucleoside dGuo characterized by weaker interactions. In particular, H-bonds between serine residues and the ligand resulted in playing a crucial role in stabilizing specific regions of the protein's structure as will be examined in detail in the section devoted to TM9 behavior.

In the case of Pt-containing compounds, a shift from the initial docked pose was further observed, most likely because of the establishment of many interactions as discussed above (see RMSD in Fig. S1). In this movement, the ligands had the opportunity to interact further with negatively charged residues, such as E344, E426, and E520 (see Fig. 4). The former, in particular, has been identified in all the trajectories with occupancies ranging from *ca.* 30–5% of occupancy. Furthermore, the radial distribution function (RDF) calculated for platinated nucleosides and negatively charged residues demonstrates that the electrostatic interaction at ∼1.8 Å is more prevalent with the platinated guanosine derivative [Pt(dien)(*N*7-dGuo)]$^{2+}$ (**1**), followed by *cis*-[Pt(NH$_3$)$_2$Cl(*N*7-dGuo)]$^{+}$ (**2**) and *cis*-[Pt(NH$_3$)$_2$(H$_2$O)(*N*7-dGuo)]$^{2+}$ (**3**). The neutral, natural nucleobase exhibits the lowest frequency (See Fig. S4).

During the simulation time, several water molecules come into interactions with the ligands, as evidenced by the analysis of the radial distribution function of O$_w$-nucleoside pairs (Fig. S5). The RDF for the presence of dGuo nucleoside shows a lower density of water molecules at shorter distances (∼3.0 Å) compared to the Pt-containing species. This indicates that water is less densely distributed around the natural nucleoside, which is engaged in H-bonds with multiple protein residues as discussed above. In the case of **1**, **2** and **3** instead, a peak at *ca.* 2.5 Å can be noticed, suggesting a higher probability of finding water molecules in proximity to metal complexes (Fig. S5). An explanation for this result resides in the shift of the species during the molecular dynamics, with Pt-containing compounds moving in proximity of the intracellular loop in proximity of TM5 (see Fig. 2) and facing a higher number of water molecules, with respect to the embedded dGuo.

Puckering of ribose moiety

The analysis of each system reveals significant features that help rationalize the experimental outcomes.[25] The structure demonstrates to be able to locate [Pt(dien)(*N*7-dGuo)]$^{2+}$ (**1**) deep within the transporter, into the nucleoside-binding site, and close to the cytoplasmic side of the membrane, regardless the presence of a very bulky moiety on *N*7. As previously discussed, the interactions can be divided into two groups: those involving the ribose moiety and those with the nucleobase. Therefore, we analyzed their behavior in terms of the contact area and of the dihedral angles in the case of the sugar ring. This allows us to highlight the conformational preference of hCNT3 with respect to the sugar ring of the natural and modified pyrimidine nucleosides examined. This aspect can cause significant differences in the binding affinities of target proteins.[53]

The conformation of the ribose moiety during the MD simulation (see Fig. 5) reveals the structural effects of the backbone in the platinated nucleosides compared with the natural one. In particular, a major rigidity of the sugar in the case of [Pt(dien)(*N*7-dGuo)]$^{2+}$ is observed, caused by its bulky group, which, pointing away from TM7 with respect to the natural dGuo, affects the ribose interactions with the transporter. The other two systems exhibit greater mobility of the ribose, in terms of puckering (Fig. S6).

In the case of Pt-containing compounds, [Pt(dien)(*N*7-dGuo)]$^{2+}$ is very bulky and is first accommodated by interacting with a number of serine residues, mainly from the TM9 domain within the pocket, as will be discussed in the next section in detail. [Pt(NH$_3$)$_2$(H$_2$O)(*N*7-dGuo)]$^{2+}$ (**3**) tends to establish interactions with water molecules and negatively charged residues more frequently. Because of such networks, the species considered can display different orientations of the ribose moiety, characterized by 3′-*endo* and 3′-*exo* conformations (or N- and S-conformation respectively, see Fig. 5).

Preliminary quantum mechanics calculations on the investigated species, including the ribose as a reference point, showed that the dihedral interchange can occur with a small

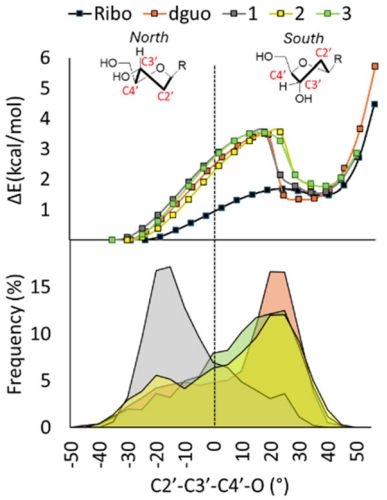

Fig. 5 Bottom: Frequency of C2′–C3′–C4′–O dihedral observed during molecular dynamics (MD) simulations. Top: Density functional theory (DFT) energy profile calculated for C2′–C3′–C4′–O dihedral for the current ligands. The following complexes are indicated in short in the picture: $[Pt(dien)(N7\text{-}dGuo)]^{2+}$ (**1**), *cis*-$[Pt(NH_3)_2Cl(N7\text{-}dGuo)]^{+}$ (**2**), and *cis*-$[Pt(NH_3)_2(H_2O)(N7\text{-}dGuo)]^{2+}$ (**3**), where dien = diethylenetriamine and dGuo = 5′-(2′-deoxy)-guanosine.

energy penalty of 1.5 kcal mol^{-1}, from N- to S-conformation (see Fig. 5). However, for the systems with a nucleobase an energy barrier of *ca.* 3.5 kcal mol^{-1} can be noticed. Interestingly, dGuo and complex **2** have a similar behaviour, with an S-conformation observed for almost the whole trajectory, while in the case of complex **1**, the N-conformation is the most populated (see Fig. 5). This set of QM calculations was performed coupling B3LYP-D3, 6-31G(d,p) basis for all atoms and the SMD implicit model (ε = 78).[54,55] Although the analysis of the energies at the QM level of theory revealed a small energy gap between the two conformations, it is interesting to note that the bulkier ligand on complex **1** imposes some limitations on the intramolecular reorganization of the structure, such as energy costless rearrangement of the ribose ring.

Behavior of the TM9 during MD

A more thorough structural analysis of the transporter segment TM9 (residues L433-F476) was carried out to deepen its role in ligand recognition and transport. As discussed above, many amino acids were found to come into contact with the ligands, with particular attention on the serine residues S442, S443, S445, and S446. A closer view of the structure of TM9 further highlighted that when the ligand lies in proximity to these serine residues, the α-helix is slightly unwound, as evidenced by the Ramachandran plots calculated for the populated clustered geometries from MD simulations reported in Fig. S7. The main reason for this conformational reorganization resides in the internal hydrogen bond networks that distinguish the TM9.

In detail, the measurements of the canonical hydrogen bonds (O–HN) between residues S443-L447 and S444-Val448 are fundamental for maintaining the structural organization of the helix. Each system shows a progressive increase in these distances, indicating the unwinding of the α-helix at these points (see Fig. 6).

Looking at the representative clustered structures obtained from the MD, in the case of the apo-form of hCNT3, the values of the H-bond distances S443-L447 and S444-V448 were 2.47 Å and 1.88 Å, in agreement with the available crystallographic structures.[34,51,52] In the hCNT3:dGuo system, the distances experience a slight change (S443-L447: 4.60 Å and S444-V448: 2.49 Å), keeping the typical values observed in a stable α-helix anyway.

In the case of hCNT3:$[Pt(dien)(N7\text{-}dGuo)]^{2+}$ system, the distance between S443 and Leu447 is measured at 6.68 Å, while the distance between S444 and V448 is 3.28 Å. These values shift from the ideal helix distances, particularly at the S444-V448 position where the distance of 3.60 Å suggests an unwound section of the helix caused by the presence of the metal complex. Similarly, in the hCNT3:*cis*-$[Pt(NH_3)_2(H_2O)(N7\text{-}dGuo)]^{2+}$ complex, the distances S444-V448 and S443-L447 were measured at 2.36 Å and 5.62 Å, respectively (see Fig. 6).

To further quantify the impact of these variations of inherent hydrogen-bond networks of the α-helix, the RMSD of TM9 (residues L433-F476) was calculated, and comparable values were observed for all the systems (Fig. S6). In addition, by investigating the length of the α-helix by measuring the head-tail distance, significant variations were not detected with respect to the apoform, with values ranging from 62–65 Å for the ligand-bound system (*ca.* 63 Å in the apo form, see Fig. S7). As a result, it was determined that TM9 can locally adjust to ligand passing-through, specifically promoting the migration of metal-containing complexes from the matrix to the intracellular environment.

The analysis of the MD simulations thus revealed the involvement of ligand-TM9 interactions, in particular of S443-V448 segment, in the migration of metal-containing species from extra- to intracellular environment, suggesting that its consideration could be relevant for design of new drugs.

The binding free energy (ΔG_{total}) values calculated using MM-PBSA (Table S2) also provide valuable insights into the stability of the systems inside the transporter channel since the considered different contributions can be strictly linked with the analysis of hydrogen bonds.

The obtained ΔG_{total} values reveal significant differences in the stability of the ligand within the membrane-protein system. The ΔG_{total} for dGuo is −31 kcal mol^{-1}, which is less negative than that of hCNT3:$[Pt(dien)(N7\text{-}dGuo)]^{2+}$ (−78.70 kcal mol^{-1}), likely due to the extended hydrogen bond network established with surrounding residues. The hCNT3:*cis*-$[Pt(NH_3)_2(H_2O)(N7\text{-}dGuo)]$ system shows a slightly negative ΔG_{total} of −4.11 kcal mol^{-1} that becomes positive +11.49 kcal mol^{-1} in hCNT3:*cis*-$[Pt(NH_3)_2Cl(N7\text{-}dGuo)]^{+}$, (Table S2) likely due to reduced H-bonds with the transporter emerged by the H-bond analysis (see Fig. 4).

Furthermore, umbrella sampling simulations able to force the exploration along a predefined reaction coordinate were

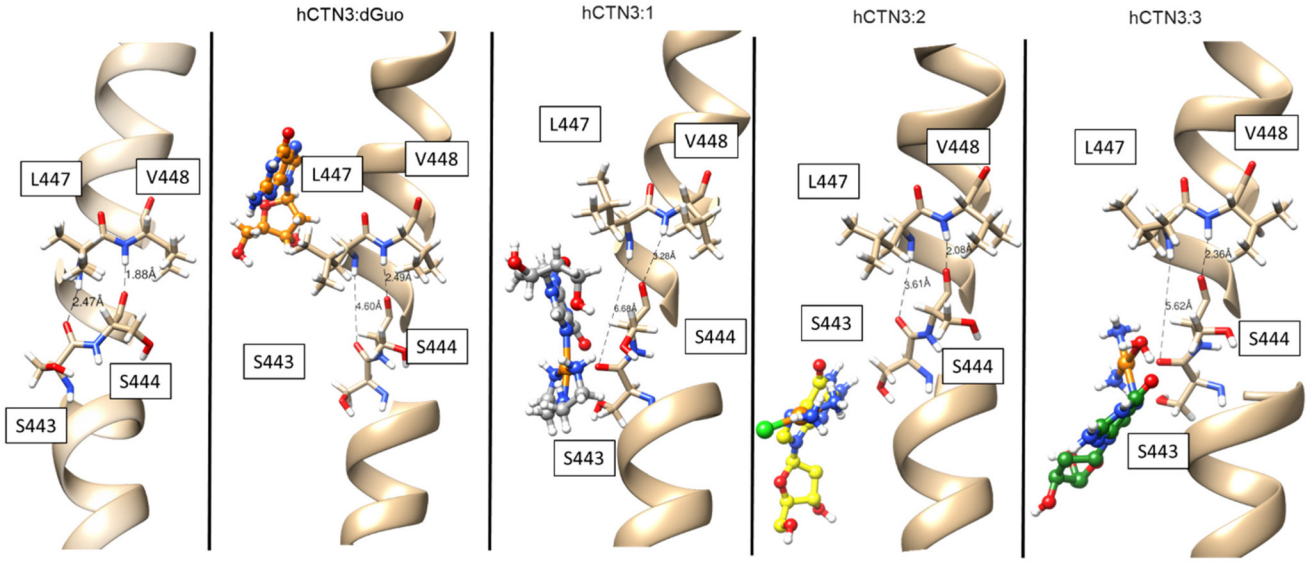

Fig. 6 Illustration of the canonical H-bonds involved in the formation of the α-helix between S443:L447 and S444:V448. The following complexes are indicated in the picture: $[Pt(dien)(N7\text{-dGuo})]^{2+}$ (**1**), *cis*-$[Pt(NH_3)_2Cl(N7\text{-dGuo})]^{+}$ (**2**), and *cis*-$[Pt(NH_3)_2(H_2O)(N7\text{-dGuo})]^{2+}$ (**3**), where dien = diethylenetriamine and dGuo = 5′-(2′-deoxy)-guanosine.

finally carried out to evaluate the energy cost of the observed movements, once the hCNT3:ligand complexes are obtained already, focusing on the energetic pathway for releasing the dGuo and *N*7-platinated complexes in the intracellular environment. Based also on the better affinity of *cis*-$[Pt(NH_3)_2(H_2O)(N7\text{-dGuo})]^{2+}$ for hCNT3 with respect to *cis*-$[Pt(NH_3)_2Cl(N7\text{-dGuo})]^{+}$, the umbrella sampling simulations were performed only on complex **1** and complex **2** in comparison to dGuo. The hydrogen bond occurring between the $-NH_2$ at the C4 position of the nucleobase and the carboxylate group of E520 (chosen as a reference point for leaving the transporter), starting from clustered geometries from MD, was the selected reaction coordinate (see Fig. 7), in order to get a reliable estimate of the potential of mean force (PMF).

The plot of PMF calculated for the dGuo-containing system clearly highlights that the existing hydrogen bond, at *ca.* 3.5 Å, stabilizes the substrate in the transporter's environment and that its cleavage requires 6 kcal mol^{-1} for releasing the nucleotide in the cell environment (see Fig. 7). Interestingly, the plot for the platinated compounds presented a different shape, with respect to the natural nucleotide. In detail, in the case of the Pt-aquo complex, a lower-energy minimum was localized at *ca.* 7.5 Å, with an almost flat energy profile in the range 2.5–4.0 Å in which the interaction should take place. In the case of the Pt-dien complex, finally, two isoenergetic minima were identified, at 6.5 Å and 7.5 Å, linked by a low energy barrier of 4 kcal mol^{-1}. This suggests that, according to the selected reaction coordinate, the hCNT3 can drive the release of considered Pt-containing compounds through the cellular membrane, due to low-energy interactions between the protein and the metal complexes, which indeed during the unbiased MD shifted from their initial position as discussed above, in

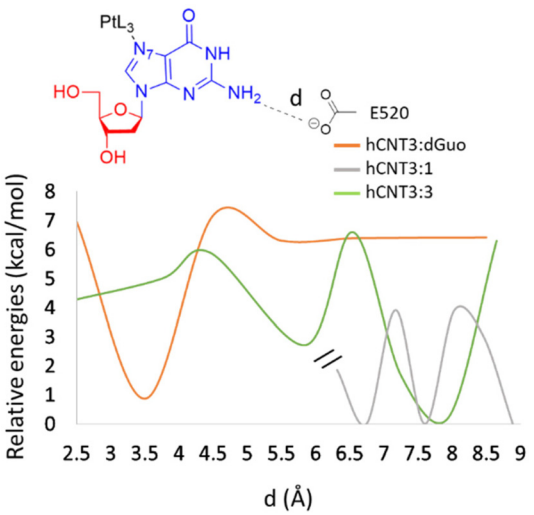

Fig. 7 Relative energies for the hydrogen bond interaction between the C4–NH_2 group of the investigated ligands and the carboxylate group of the E520 residue, obtained from umbrella sampling (US) simulations. The following complexes are indicated in the picture: $[Pt(dien)(N7\text{-dGuo})]^{2+}$ (**1**, PtL_3 = Pt(dien)), *cis*-$[Pt(NH_3)_2Cl(N7\text{-dGuo})]^{+}$ (**2**, PtL_3 = Pt$(NH_3)_2Cl$), and *cis*-$[Pt(NH_3)_2(H_2O)(N7\text{-dGuo})]^{2+}$ (**3**, PtL_3 = Pt$(NH_3)_2(H_2O)$), where dien = diethylenetriamine and dGuo = 5′-(2′-deoxy)-guanosine.

agreement with experimental results.[23] This can be justified mainly considering the bulky nature of Pt-containing arms of the complexes that branch off from *N*7 position of the nucleobase. Remarkably, for dien-containing complex it was not possible to investigate the PMF region at shorter distances (from 2.5 to 6 Å), due to the bulky nature of the ligand that does not allow any conformational reorganization of the molecule. This structural analysis, together with the energy behav-

ior discussed above, highlights how the protein channel crossing of complex **1** can occur at low energy cost, thus ensuring the pass trough of the molecule in cellular environment. This aspect is nicely in line with the experimental outcomes and helps the rationalization of results from the cellular assays previously performed, in which the highest uptake by HeLa cells resulted for complex **1**, with respect to $[Pt(dien)(N7\text{-dGTP})]^{2-}$ and [Pt(dien)(*N*7-dGMP)] species.[23]

Conclusions

This study provides insights into the interactions of *N*7-platinated guanosines with the hCNT3 transporter through molecular dynamics, highlighting their potential as therapeutic agents. Distinct behaviors were observed among the considered platinated derivatives, with $[Pt(dien)(N7\text{-dGuo})]^{2+}$ (**1**) exhibiting a more hydrophobic nature compared to *cis*-$[Pt(NH_3)_2Cl(N7\text{-dGuo})]^{+}$ (**2**) and *cis*-$[Pt(NH_3)_2(H_2O)(N7\text{-dGuo})]^{2+}$ (**3**). The results align well with experimental observations regarding the uptake of **1** at the plasma membrane level, suggesting hCNT3 as a potential transporter for this and related platinated species. The conformational changes observed for **1** compared to dGuo could be associated with their different steps along the transport cycle, as also observed for complexes **2** and **3**.

Several structural aspects of hCNT3 in the presence of complexes **1**–**3** were analyzed. Key mechanistic insights reveal that the platinated nucleosides alter the dynamics of the transporter, particularly in the intracellular loop and TM9 helix, leading to decreased flexibility and structural reorganization. This reduced flexibility may hinder nucleoside transport, highlighting the potential of these compounds to modulate transporter activity. Water molecules and hydrogen bonding were found to play significant roles in stabilizing the interactions, enhancing the inhibitory properties of **1**–**3** derivatives.

The findings propose a novel perspective based on the inhibitory potential of *N*7-platinated purine nucleoside derivatives, which could modulate the uptake of nucleosides at the cellular membrane level. These findings suggest that the previously tested complex **2** and its analogues could generate cytotoxicity in cancer cells not only by a classical mechanism involving interactions with cellular DNA, but also through a synergistic inhibitory activity affecting the activity of nucleoside transporters localized in the plasma membrane. Healthy cells are expected to be less sensitive to a decrease in the uptake of semi-essential nucleosides.[16]

This dual parallel mechanism could explain the observed low to moderate cytotoxicity associated with enhanced selectivity towards cancer cells, compared to healthy cells, recently observed on different cell lines for complexes in the series of *cis*-$[Pt(NH_3)_2X(N7\text{-Guo/dGuo})]^{+}$ (X = halido ligand) derivatives.[29] A role of Organic Cation Transporters (OCT) previously found to be responsible for the cell uptake of the Phenanthriplatin (*cis*-$[Pt(NH_3)_2Cl(\text{phenanthridine})]^{+}$) antitumor drug cannot be excluded even for *cis*-$[Pt(NH_3)_2X(N7\text{-Guo/dGuo})]^{+}$ (X = halido ligand) derivatives, due to the same positive charge and high structural similarities.[56]

Overall, this work underscores the potential of platinum-based modifications to enhance antitumor therapies based on nucleoside analogs by synergistically targeting hCNT transporters, metabolic pathways of natural nucleosides, and DNA functionality. Notably, the latter two interactions, in the case of complexes **2** and **3**, could also produce the classical 1,2-intrastrand cross-link lesions with DNA, which are responsible for the antitumor activity of cisplatin and analogous complexes.[17] These considerations could lay the groundwork for new strategies aimed at developing antitumor drugs characterized by enhanced antitumor activity, selectivity for tumor cells, and lower systemic side effects.

The exploration of platinated nucleosides within the context of nucleoside transporters presents a novel and promising strategy for cancer chemotherapy.[57–59] This dual-function approach utilizes the specific uptake pathways of nucleoside transporters, enabling platinated nucleosides to overcome some limitations of classical platinum agents such as cisplatin, which primarily depend on DNA binding.[17] This strategy combines the targeted nature of nucleoside analogues, selectively taken up by rapidly dividing cells *via* nucleoside transporters, with the potent cytotoxic properties of platinum drugs. The outcome is a multifunctional therapeutic entity that not only enhances selective drug delivery and potentially minimizes systemic toxicity but also bypasses some common resistance mechanisms associated with traditional platinum treatments. Despite its higher selectivity for cancer cells, *cis*-$[Pt(NH_3)_2Cl(N7\text{-dGuo})]^{+}$ is less cytotoxic than cisplatin.[24] This is likely due to the presence of only one leaving chlorido ligand in its coordination sphere, compared to the two found in cisplatin, an aspect that could contribute to a reduction in unwanted side effects.

Conflicts of interest

There are no conflicts to declare.

Data availability

The data supporting this article have been included as part of the SI. Docking results and additional analysis of Molecular Dynamics simulations. Supplementary information is available. See DOI: **https://doi.org/10.1039/d5qi01630d**.

Acknowledgements

Financial support from Dipartimento di Chimica e Tecnologie Chimiche, Università della Calabria, is acknowledged. Some of the computer simulations were carried out adopting resources of the supercomputer Leonardo (HP10CWFXS1) from ISCRA and from CRESCO/ENEAGRID High-Performance Computing infrastructure and its staff. CRESCO/ENEAGRID High Performance Computing infrastructure is funded by ENEA, the

Italian National Agency for New Technologies, Energy and Sustainable Economic Development and by Italian and European research programs, see **https://www.cresco.enea.it/english** for information.[60]

References

1 J. D. Young, The SLC28 (CNT) and SLC29 (ENT) Nucleoside Transporter Families: A 30-Year Collaborative Odyssey, *Biochem. Soc. Trans.*, 2016, **44**(3), 869–876, DOI: **10.1042/BST20160038**.

2 A. E. King, M. A. Ackley, C. E. Cass, J. D. Young and S. A. Baldwin, Nucleoside Transporters: From Scavengers to Novel Therapeutic Targets, *Trends Pharmacol. Sci.*, 2006, **27**(8), 416–425, DOI: **10.1016/j.tips.2006.06.004**.

3 T. W. Traut, Physiological Concentrations of Purines and Pyrimidines, *Mol. Cell. Biochem.*, 1994, **140**(1), 1–22, DOI: **10.1007/BF00928361**.

4 V. L. Damaraju, S. Damaraju, J. D. Young, S. A. Baldwin, J. Mackey, M. B. Sawyer and C. E. Cass, Nucleoside Anticancer Drugs: The Role of Nucleoside Transporters in Resistance to Cancer Chemotherapy, *Oncogene*, 2003, **22**(47), 7524–7536, DOI: **10.1038/sj.onc.1206952**.

5 K. D. Ibarra and J. K. Pfeiffer, Reduced Ribavirin Antiviral Efficacy via Nucleoside Transporter-Mediated Drug Resistance, *J. Virol.*, 2009, **83**(9), 4538–4547, DOI: **10.1128/JVI.02280-08**.

6 V. Molho-Pessach, I. Lerer, D. Abeliovich, Z. Agha, A. Abu Libdeh, V. Broshtilova, O. Elpeleg and A. Zlotogorski, The H Syndrome Is Caused by Mutations in the Nucleoside Transporter HENT3, *Am. J. Hum. Genet.*, 2008, **83**(4), 529–534, DOI: **10.1016/j.ajhg.2008.09.013**.

7 J. de Jesus, Z. Imane, V. Senée, S. Romero, P.-J. Guillausseau, A. Balafrej and C. Julier, SLC29A3 Mutation in a Patient with Syndromic Diabetes with Features of Pigmented Hypertrichotic Dermatosis with Insulin-Dependent Diabetes, H Syndrome and Faisalabad Histiocytosis, *Diabetes Metab.*, 2013, **39**(3), 281–285, DOI: **10.1016/j.diabet.2013.03.007**.

8 P. C. Preusch, Equilibrative and Concentrative Transport Mechanisms. in *Principles of Clinical Pharmacology*, Elsevier, 2007; pp 197–227. DOI: **10.1016/B978-012369417-1/50054-7**.

9 R. C. Boswell-Casteel and F. A. Hays, Equilibrative Nucleoside Transporters—A Review, *Nucleosides, Nucleotides Nucleic Acids*, 2017, **36**(1), 7–30, DOI: **10.1080/15257770.2016.1210805**.

10 J. H. Gray, R. P. Owen and K. M. Giacomini, The Concentrative Nucleoside Transporter Family, SLC28, *Pfluegers Arch.*, 2004, **447**(5), 728–734, DOI: **10.1007/s00424-003-1107-y**.

11 P. Cano–Soldado and M. Pastor–Anglada, Transporters That Translocate Nucleosides and Structural Similar Drugs: Structural Requirements for Substrate Recognition, *Med. Res. Rev.*, 2012, **32**(2), 428–457, DOI: **10.1002/med.20221**.

12 I. Badagnani, W. Chan, R. A. Castro, C. M. Brett, C. C. Huang, D. Stryke, M. Kawamoto, S. J. Johns, T. E. Ferrin, E. J. Carlson, E. G. Burchard and K. M. Giacomini, Functional Analysis of Genetic Variants in the Human Concentrative Nucleoside Transporter 3 (CNT3; SLC28A3), *Pharmacogenomics J.*, 2005, **5**(3), 157–165, DOI: **10.1038/sj.tpj.6500303**.

13 M. Molina-Arcas, F. Casado and M. Pastor-Anglada, Nucleoside Transporter Proteins, *Curr. Vasc. Pharmacol.*, 2009, **7**(4), 426–434, DOI: **10.2174/157016109789043892**.

14 R. A. Hesler, J. J. Huang, M. D. Starr, V. M. Treboschi, A. G. Bernanke, A. B. Nixon, S. J. McCall, R. R. White and G. C. Blobe, TGF-β-Induced Stromal CYR61 Promotes Resistance to Gemcitabine in Pancreatic Ductal Adenocarcinoma through Downregulation of the Nucleoside Transporters HENT1 and HHCNT3, *Carcinogenesis*, 2016, **37**(11), 1041–1051, DOI: **10.1093/carcin/bgw093**.

15 M. W. L. Ritzel, A. M. L. Ng, S. Y. M. Yao, K. Graham, S. K. Loewen, K. M. Smith, R. G. Ritzel, D. A. Mowles, P. Carpenter, X.-Z. Chen, E. Karpinski, R. J. Hyde, S. A. Baldwin, C. E. Cass and J. D. Young, Molecular Identification and Characterization of Novel Human and Mouse Concentrative Na+-Nucleoside Cotransporter Proteins (CNT3 and MCNT3) Broadly Selective for Purine and Pyrimidine Nucleosides (System Cib), *J. Biol. Chem.*, 2001, **276**(4), 2914–2927, DOI: **10.1074/jbc.M007746200**.

16 G. Ferrandina, V. Mey, S. Nannizzi, S. Ricciardi, M. Petrillo, C. Ferlini, R. Danesi, G. Scambia and M. Del Tacca, Expression of Nucleoside Transporters, Deoxycitidine Kinase, Ribonucleotide Reductase Regulatory Subunits, and Gemcitabine Catabolic Enzymes in Primary Ovarian Cancer, *Cancer Chemother. Pharmacol.*, 2010, **65**(4), 679–686, DOI: **10.1007/s00280-009-1073-y**.

17 T. C. Johnstone, K. Suntharalingam and S. J. Lippard, The Next Generation of Platinum Drugs: Targeted Pt(II) Agents, Nanoparticle Delivery, and Pt(IV) Prodrugs, *Chem. Rev.*, 2016, **116**(5), 3436–3486, DOI: **10.1021/acs.chemrev.5b00597**.

18 F. Arnesano and G. Natile, Mechanistic Insight into the Cellular Uptake and Processing of Cisplatin 30 Years after Its Approval by FDA, *Coord. Chem. Rev.*, 2009, **253**(15–16), 2070–2081, DOI: **10.1016/j.ccr.2009.01.028**.

19 B. Rosenberg, Fundamental Studies with Cisplatin, *Cancer*, 1985, **55**(10), 2303–2316, DOI: **10.1002/1097-0142(19850515)55:10<2303::AID-CNCR2820551002>3.0.CO;2-L**.

20 B. Rosenberg, Platinum Complexes for the Treatment of Cancer: Why the Search Goes On. in *Cisplatin*, Wiley, 1999, pp 1–27. DOI: **10.1002/9783906390420.ch1**.

21 C. M. Galmarini, J. R. Mackey and C. Dumontet, Nucleoside Analogues and Nucleobases in Cancer Treatment, *Lancet Oncol.*, 2002, **3**(7), 415–424, DOI: **10.1016/S1470-2045(02)00788-X**.

22 L. P. Jordheim, D. Durantel, F. Zoulim and C. Dumontet, Advances in the Development of Nucleoside and Nucleotide Analogues for Cancer and Viral Diseases, *Nat.*

Rev. Drug Discovery, 2013, **12**(6), 447–464, DOI: **10.1038/nrd4010**.

23 F. De Castro, E. De Luca, C. R. Girelli, A. Barca, A. Romano, D. Migoni, T. Verri, M. Benedetti and F. P. Fanizzi, First Evidence for N7-Platinated Guanosine Derivatives Cell Uptake Mediated by Plasma Membrane Transport Processes, *J. Inorg. Biochem.*, 2022, **226**, 111660, DOI: **10.1016/j.jinorgbio.2021.111660**.

24 A. Ali, G. Rovito, E. Stefàno, F. De Castro, G. Ciccarella, D. Migoni, E. Panzarini, A. Muscella, S. Marsigliante, M. Benedetti, *et al.* Synthesis, Structural Characterization, and Cytotoxic Evaluation of Monofunctional Cis-[Pt(NH3)2 (N7-Guanosine/2′-Deoxyguanosine)X] (X = Cl, Br, I) Complexes with Anticancer Potential, *Dalton Trans.*, 2025, **54**, 8612–8624, DOI: **10.1039/D5DT00616C**.

25 M. Benedetti, C. Ducani, D. Migoni, D. Antonucci, V. M. Vecchio, A. Ciccarese, A. Romano, T. Verri, G. Ciccarella and F. P. Fanizzi, Experimental Evidence That a DNA Polymerase Can Incorporate N7−Platinated Guanines To Give Platinated DNA, *Angew. Chem., Int. Ed.*, 2008, **47**(3), 507–510, DOI: **10.1002/anie.200703160**.

26 P. Lunetti, A. Romano, C. Carrisi, D. Antonucci, T. Verri, G. E. De Benedetto, V. Dolce, F. P. Fanizzi, M. Benedetti and L. Capobianco, latinated Nucleotides Are Substrates for the Human Mitochondrial Deoxynucleotide Carrier (DNC) and DNA Polymerase γ: Relevance for the Development of New Platinum–Based Drugs, *ChemistrySelect*, 2016, **1**(15), 4633–4637, DOI: **10.1002/slct.201600961**.

27 F. De Castro, E. Stefàno, E. De Luca, M. Benedetti and F. P. Fanizzi, Platinum-Nucleos(t)Ide Compounds as Possible Antimetabolites for Antitumor/Antiviral Therapy: Properties and Perspectives, *Pharmaceutics*, 2023, **15**(3), 941, DOI: **10.3390/pharmaceutics15030941**.

28 M. Benedetti, A. Romano, F. De Castro, C. R. Girelli, D. Antonucci, D. Migoni, T. Verri and F. P. Fanizzi, N7-Platinated Ribonucleotides Are Not Incorporated by RNA Polymerases. New Perspectives for a Rational Design of Platinum Antitumor Drugs, *J. Inorg. Biochem.*, 2016, **163**, 143–146, DOI: **10.1016/j.jinorgbio.2016.07.004**.

29 F. De Castro, G. Ciardullo, F. P. Fanizzi, M. Prejanò, M. Benedetti and T. Marino, Incorporation of N7-Platinated Guanines into Thermus Aquaticus (Taq) DNA Polymerase: Atomistic Insights from Molecular Dynamics Simulations, *Int. J. Mol. Sci.*, 2023, **24**(12), 9849, DOI: **10.3390/ijms24129849**.

30 M. Benedetti, D. Antonucci, F. De Castro, C. R. Girelli, M. Lelli, N. Roveri and F. P. Fanizzi, Metalated Nucleotide Chemisorption on Hydroxyapatite, *J. Inorg. Biochem.*, 2015, **153**, 279–283, DOI: **10.1016/j.jinorgbio.2015.04.006**.

31 C. Carrisi, D. Antonucci, P. Lunetti, D. Migoni, C. R. Girelli, V. Dolce, F. P. Fanizzi, M. Benedetti and L. Capobianco, Transport of Platinum Bonded Nucleotides into Proteoliposomes, Mediated by *Drosophila Melanogaster* Thiamine Pyrophosphate Carrier Protein (*Dm*Tpc1), *J. Inorg. Biochem.*, 2014, **130**, 28–31, DOI: **10.1016/j.jinorgbio.2013.09.012**.

32 M. Benedetti, C. Ducani, D. Migoni, D. Antonucci, V. M. Vecchio, A. Romano, T. Verri and F. P. Fanizzi, Possible Incorporation of Free N7-Platinated Guanines in DNA by DNA Polymerases, Relevance for the Cisplatin Mechanism of Action, in *Platinum and Other Heavy Metal Compounds in Cancer Chemotherapy: Molecular Mechanisms and Clinical Applications*, ed. A. Bonetti, R. Leone, F. M. Muggia and S. B. Howell, Cancer Drug Discovery and Development, Humana Press, Totowa, NJ, 2009, pp. 125–132, ISBN 978-1-60327-459-3.

33 L. S. Hollis, A. R. Amundsen and E. W. Stern, Chemical and Biological Properties of a New Series of Cis-Diammineplatinum(II) Antitumor Agents Containing Three Nitrogen Donors: Cis-[Pt(NH3)2(N-Donor) Cl]+, *J. Med. Chem.*, 1989, **32**, 128–136, DOI: **10.1021/jm00121a024**.

34 Y. Zhou, L. Liao, C. Wang, J. Li, P. Chi, Q. Xiao, Q. Liu, L. Guo, L. Sun and D. Deng, Cryo-EM Structure of the Human Concentrative Nucleoside Transporter CNT3, *PLoS Biol.*, 2020, **18**(8), e3000790, DOI: **10.1371/journal.pbio.3000790**.

35 R. Dennington, T. Keith and J. Millam, *GaussView, Version 6.1.1*, Semichem Inc., Shawnee Mission, KS, 2019.

36 P. Li and K. M. Merz, MCPB.Py: A Python Based Metal Center Parameter Builder, *J. Chem. Inf. Model.*, 2016, **56**(4), 599–604, DOI: **10.1021/acs.jcim.5b00674**.

37 M. J. Frisch, G. W. Trucks, H. B. Schlegel, G. E. Scuseria, M. A. Robb, J. R. Cheeseman, G. Scalmani, V. Barone, G. A. Petersson and H. Nakatsuji, *Gaussian 16, Revision C. 01*, Gaussian, Inc., Wallingford CT, 2016.

38 A. D. Becke, Density-Functional Thermochemistry, III. The Role of Exact Exchange, *J. Chem. Phys.*, 1993, **98**(7), 5648–5652, DOI: **10.1063/1.464913**.

39 C. Lee, W. Yang and R. G. Parr, Development of the Colle-Salvetti Correlation-Energy Formula into a Functional of the Electron Density, *Phys. Rev. B:Condens. Matter Mater. Phys.*, 1988, **37**(2), 785–789, DOI: **10.1103/PhysRevB.37.785**.

40 D. A. Case, R. C. Walker, T. Darden and J. Wang, *Amber 2016 Reference Manual Principal Contributors to the Current Codes*. **https://ambermd.org/contributors.html**.

41 C. I. Bayly, P. Cieplak, W. Cornell and P. A. Kollman, A Well-Behaved Electrostatic Potential Based Method Using Charge Restraints for Deriving Atomic Charges: The RESP Model, *J. Phys. Chem.*, 1993, **97**(40), 10269–10280, DOI: **10.1021/j100142a004**.

42 G. M. Morris, R. Huey, W. Lindstrom, M. F. Sanner, R. K. Belew, D. S. Goodsell and A. J. Olson, AutoDock4 and AutoDockTools4: Automated Docking with Selective Receptor Flexibility, *J. Comput. Chem.*, 2009, **30**(16), 2785–2791, DOI: **10.1002/jcc.21256**.

43 J. Gasteiger and M. Marsili, Iterative Partial Equalization of Orbital Electronegativity—a Rapid Access to Atomic Charges, *Tetrahedron*, 1980, **36**(22), 3219–3228, DOI: **10.1016/0040-4020(80)80168-2**.

44 S. Jo, T. Kim, V. G. Iyer and W. Im, CHARMM–GUI: A Web–based Graphical User Interface for CHARMM, *J. Comput. Chem.*, 2008, **29**(11), 1859–1865, DOI: **10.1002/jcc.20945**.

45 D. Casares, P. V. Escribá and C. A. Rosselló, Membrane Lipid Composition: Effect on Membrane and Organelle Structure, Function and Compartmentalization and Therapeutic Avenues, *Int. J. Mol. Sci*, 2019, **20**(9), 2167, DOI: **10.3390/ijms20092167**.

46 J. Wang, R. M. Wolf, J. W. Caldwell, P. A. Kollman and D. A. Case, Development and Testing of a General Amber Force Field, *J. Comput. Chem.*, 2004, **25**(9), 1157–1174, DOI: **10.1002/jcc.20035**.

47 C. J. Dickson, B. D. Madej, Å.A Skjevik, R. M. Betz, K. Teigen, I. R. Gould and R. C. Walker, Lipid14: The Amber Lipid Force Field, *J. Chem. Theory Comput.*, 2014, **10**(2), 865–879, DOI: **10.1021/ct4010307**.

48 M. J. Abraham, T. Murtola, R. Schulz, S. Páll, J. C. Smith, B. Hess and E. Lindahl, GROMACS: High Performance Molecular Simulations through Multi-Level Parallelism from Laptops to Supercomputers, *SoftwareX*, 2015, **1–2**, 19–25, DOI: **10.1016/j.softx.2015.06.001**.

49 D. Van Der Spoel, E. Lindahl, B. Hess, G. Groenhof, A. E. Mark and H. J. C. Berendsen, GROMACS: Fast, Flexible, and Free, *J. Comput. Chem.*, 2005, **26**(16), 1701–1718, DOI: **10.1002/jcc.20291**.

50 T. Nagai, A. Mitsutake and H. Takano, Principal Component Relaxation Mode Analysis of an All-Atom Molecular Dynamics Simulation of Human Lysozyme, *J. Phys. Soc. Jpn.*, 2013, **82**(2), 023803, DOI: **10.7566/JPSJ.82.023803**.

51 Z. L. Johnson, C.-G. Cheong and S.-Y. Lee, Crystal structure of a concentrative nucleoside transporter from Vibrio cholerae at 2.4 Å, *Nature*, 2012, **483**, 489–493.

52 N. J. Wright, F. Zhang, Y. Suo, L. Kong, Y. Yin, J. G. Fedor, K. Shrma, M. J. Borgna, W. Im and S.-Y. Lee, Antiviral drug recognition and elevator-type transport motions of CNT3, *Nat. Chem. Biol.*, 2024, 1144–1153.

53 V. L. Damaraju, D. Mowles, K. M. Smith, S. Y. M. Yao, J. D. Young, V. E. Marquez and C. E. Cass, Influence of sugar ring conformation on the transportability of nucleosides by human nucleoside transporters, *ChemBioChem*, 2011, **12**, 2774–2778.

54 S. Grimme, J. Antony, S. Ehrlich and H. Krieg, A consistent and accurate ab initio parametrization of density functional dispersion correction (DFT-D) for the 94 elements H-Pu, *J. Chem. Phys.*, 2010, **132**, 154104.

55 S. Grimme, S. Ehrlich and L. Goerigk, Effect of the damping function in dispersion corrected density functional theory, *J. Comput. Chem.*, 2011, **32**, 1456–1465.

56 A. Hucke, G. Y. Park, O. B. Bauer, G. Beyer, C. Köppen, D. Zeeh, C. A. Wehe, M. Sperling, R. Schröter, M. Kantauskaitè, Y. Hagos and U. Karst, Lippard SJ and Ciarimboli G Interaction of the New Monofunctional Anticancer Agent Phenanthriplatin With Transporters for Organic Cations, *Front. Chem.*, 2018, **6**, 180, DOI: **10.3389/fchem.2018.00180**.

57 C. A. Koczor, R. A. Torres and W. Lewis, The role of transporters in the toxicity of nucleoside and nucleotide analogs. Expert Opin. Drug Metab, *Toxicology*, 2012, **8**(6), 665–676.

58 M. Pastor-Anglada and S. Pérez-Torras, Emerging Roles of Nucleoside Transporters, *Front. Pharmacol.*, 2018, **9**, 606.

59 J. Zhang, F. Visser, K. M. King, S. A. Baldwin, J. D. Young and C. E. Cass, The role of nucleoside transporters in cancer chemotherapy with nucleoside drugs, *Cancer Metastasis Rev.*, 2007, **26**(1), 85–110.

60 F. Iannone, F. Ambrosino, G. Bracco, M. De Rosa, A. Funel, G. Guarnieri, S. Migliori, F. Palombi, G. Ponti, S. Santomauro and P. Procacci, *International Conference on High Performance Computing and Simulation (HPCS)*, Dublin, Ireland, 2019, pp. 1051–1052.

